Open Access

Journal of Energy and Power Technology

LIDSEN Publishing Inc.

Original Research

The Effect of Rotor Radius Ratio on The Performance of Hybrid Vertical Axis Wind Turbine Savonius-Darrieus NREL S809

Elysa Nensy Irawan [1, 2, †], Sandro Sitompul [1, †], Ken-Ichiro Yamashita [3, †], Goro Fujita [1, †, *]

1. Department of Electrical Engineering, Shibaura Institute of Technology, Tokyo, Japan; E-Mails: nb22502@shibaura-it.ac.jp; i046099@shibaura-it.ac.jp; gfujita@sic.shibaura-it.ac.jp
2. Department of Mechatronics and Artificial Intelligence, Universitas Pendidikan Indonesia, Bandung, Indonesia
3. Department of Electrical Engineering, Salesian Polytechnic, Tokyo, Japan; E-Mail: yamasita@salesio-sp.ac.jp

† These authors contributed equally to this work.

* **Correspondence:** Goro Fujita; E-Mail: gfujita@sic.shibaura-it.ac.jp

Academic Editor: Andrés Elías Feijóo Lorenzo

Collection: Wind Energy

Journal of Energy and Power Technology
2023, volume 5, issue 1
doi:10.21926/jept.2301001

Received: October 05, 2022
Accepted: December 20, 2022
Published: January 02, 2023

Abstract

This research aims to know the effect of the Rotor Radius Ratio on the performance of the hybrid Vertical Axis Wind Turbine Savonius-Darrieus NREL S809 model using the Computational Fluid Dynamics method. Two-bladed Savonius is used as an internal rotor, and three-bladed Darrieus NREL S809 as an external rotor. Turbine model performance is analyzed through the value of the Moment Coefficient and Power Coefficient. The result shows that the increase in the Rotor Radius Ratio value causes an increase in the initial Moment Coefficient but a decrease in the maximum Power Coefficient value. At the initial TSR, the Rotor Radius Ratio 0.5 model has the best Moment Coefficient value among all variations but has the lowest maximum Power Coefficient value.

Keywords

Computational fluid dynamics; hybrid vertical axis wind turbine; NREL S809; moment coefficient; power coefficient; rotor radius ratio; tip speed ratio

1. Introduction

During the Covid-19 era, global energy consumption has decreased [1]. However, in 2021, energy consumption increased again by 4% from the previous year [2]. So far, the most widely used energy source globally is fossil energy [3]. Even in 2007, 80% of the total energy demand in the world was still dominated by fossil energy [4]. Because the use of fossil energy can cause CO_2 emissions that lead to global warming [5], starting in 2010 until now, the use of fossil energy continues to be reduced and replaced by renewable energy [6]. The development of renewable energy from 2001 to 2020 continues to increase; even in 2020, there was an increase of 29% from 2019 [6]. Efforts to increase renewable energy will continue to be intensified using implementation in various fields, such as industry [7], transportation [8], and so on.

Renewable energy sources can be obtained from the natural surroundings, like hydrothermal, geothermal, solar, wind, marine, and biogenic energies [9]. Among all these renewable energy sources, one of the renewable energies that have the potential to be developed is wind energy. According to [10], more than 50% of renewable energy in the world is dominated by wind energy. Especially in ASEAN, many regions have considerable wind energy potential [10].

Wind energy can be converted into electrical energy using a wind turbine [11]. There are two types of wind turbines, namely Horizontal Axis Wind Turbines (HAWT) and Vertical Axis Wind turbines (VAWT) [11]. According to [12], VAWT has more advantages than HAWT. VAWT consists of several types with their respective performances based on Power Coefficient (C_P) graph, as shown in Figure 1.

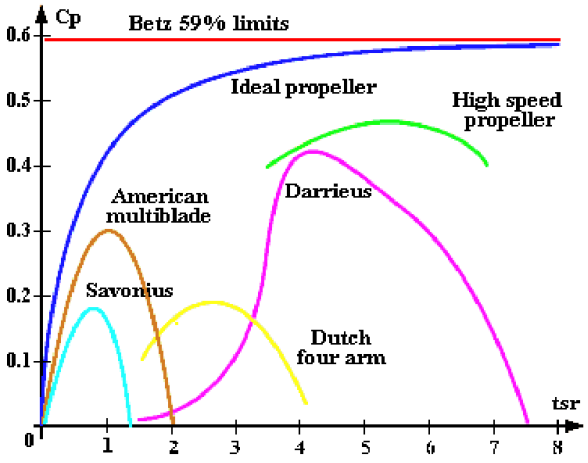

Figure 1 Graph of Power Coefficient (C_P) of several types of VAWT [13].

The graph in Figure 1 is important for understanding the basic performance of wind turbines. The blue line shows the ideal efficiency of the HAWT, while the others are various types of VAWT. Among all the VAWT types, the most popular types are Savonius and Darrieus. Savonius works using the

drag force principle, while Darrieus uses the lift force principle [14]. Darrieus has a higher C_P than Savonius but requires a higher wind speed to start the rotation than Savonius [15]. Therefore, many researchers combine Savonius and Darrieus (hybrid Savonius-Darrieus) to take advantage of Savonius and Darrieus.

Using the hybrid Savonius-Darrieus cannot increase the initial torque and the Savonius and cannot produce the C_P as well as Darrieus [16]. The performance of the hybrid Savonius-Darrieus is the interference of the two properties of the turbine. To improve the performance of the hybrid Savonius-Darrieus, the researchers studied several influential aspects such as the position of the turbine arrangement, the barrier walls provided on the side of the returning blade, the overlap ratio, the type of airfoil, the rotor radius ratio, and so on.

[17] conducted experimental research and Computational Fluid Dynamics (CFD) to determine the effect of turbine arrangement position on the performance of hybrid Savonus-Darrieus. As a result, the Darrieus turbine mounted on the Savonius with a phase angle of 0° has the best performance among others. At a wind speed of 3 m/s, the turbine model has a Moment Coefficient (C_M) of 0.303 and a C_P of 0.3195. [18] conducted a CFD study to improve the performance of the hybrid Savonius-Darrieus by placing a barrier wall on the side of the Savonius returning blades to reduce the negative torque generated by Savonius. However, this method is not optimal because it is only effective for one direction of fluid flow. [19] conducted a CFD study on the effect of the overlap ratio of Savonius on the performance of the hybrid Savonius-Darrieus. As a result, increasing the overlap ratio can increase turbine self-starting, and an overlap ratio of 2.5 can increase C_P by 18% from the basic hybrid Savonius-Darrieus model. [20] conducted a study to determine the effect of the type of airfoil on the performance of the hybrid Savonius-Darrieus. Based on the results of his research, the asymmetrical airfoil gives a better C_P than the symmetrical airfoil. However, changing the airfoil does not significantly impact the initial torque value of the hybrid turbine. Another way that can be done to improve VAWT performance is augmentation techniques, as described in the article [21]. hat article also explains that airfoil modification can save costs, but the other benefits will be very small.

[22] conducted a study on the effect of the Savonius-Darrieus height ratio on the performance of the hybrid Savonius-Darrieus. As a result, the increase in the Savonius-Darrieus height ratio gives a fairly linear result to the increase in turbine torque. The turbine model with a ratio of 1.4 is the best and can increase the initial torque of the turbine by 48% compared to a single Darrieus. Based on this research, it is possible to increase the initial torque of the hybrid Savonius-Darrieus by adjusting the rotor radius ratio. The rotor radius ratio (R_S/R_D) is the ratio of the Savonius and Darrieus radii in the hybrid Savonius-Darrieus. Experimental research on the effect of the R_S/R_D has been carried out by [23] using a symmetrical NACA 0020 airfoil. However, CFD research on the effect of the R_S/R_D on the performance of the hybrid Savonius-Darrieus has never been done. So, on this occasion, a CFD analysis was carried out to find out the effect of R_S/R_D on the performance of the hybrid Savonius-Darrieus using the NREL S809 asymmetrical airfoil because, based on research [24], NREL S809 has a better maximum Power Coefficient (C_{Pmax}) value compared to symmetrical airfoils and some asymmetrical airfoils.

2. Materials and Methods

2.1 Preprocessing

This research was conducted using the CFD method. This CFD uses Reynolds-Averaged Navier Stokes (RANS) equations as follows.

Continuity

$$\frac{\partial \bar{\rho}}{\partial t} + \overline{\nabla \cdot u} = 0 \tag{1}$$

x-momentum

$$-\nabla \bar{P} + \mu \nabla^2 \bar{u} + \rho g = \rho \left(\frac{\partial \bar{u}}{\partial t} + \bar{u} \cdot \nabla \bar{u} \right) + \nabla RS \tag{2}$$

y-momentum

$$-\nabla \bar{P} + \mu \nabla^2 \bar{y} + \rho g = \rho \left(\frac{\partial v}{\partial t} + \bar{v} \cdot \nabla \bar{v} \right) + \nabla RS \tag{3}$$

ρ is fluid density (kg/m^3), u is wind velocity (m/s), P is fluid pressure (Pa), μ is the dynamic fluid viscosity (kg/m·s), v is the fluid kinematic viscosity (m^2/s), S is training (N/m), ∇ indicates the gradient differential operator, and $\nabla^2$is the Laplacian operator. The RANS equations can describe the phenomenon of fluid flow and explain the balance of forces acting on the fluid [25] so that these fit the needs of this research.

There are three stages in CFD, namely preprocessing, processing, and postprocessing. This CFD is done by using Ansys Fluent 18.1 software. The preprocessing stage includes creating geometry, creating boundary conditions, and meshing. This hybrid turbine model uses Savonius as an internal rotor and Daerrieus as an external rotor. The configuration of the hybrid VAWT Savonius-Darrieus NREL S809 model used is shown in Table 1.

Table 1 Configuration of the hybrid VAWT Savonius-Darrieus NREL S809 model.

Hybrid VAWT Savonius-Darrieus NREL S809 Configuration	
Savonius	
Number of blades	2
Overlap ratio	0
Aspect ratio (H/D)	0.77
Blade arc angle	135°
Darrieus	
Airfoil	NREL S809
Number of blades	3
R_D	30 cm
Solidity	0.5
Hybrid	
Rotor Radius Ration (R_S/R_D)	0.1 – 0.5

Angle of attack	15°

The 3D view of the model is show in Figure 2.

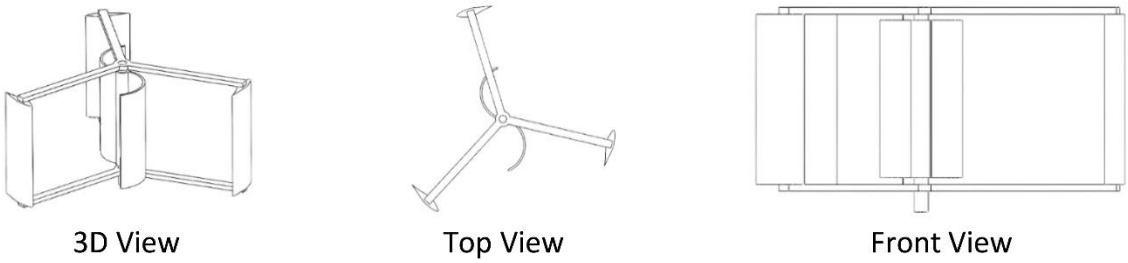

Figure 2 Hybrid VAWT Savonius-Darrieus NREL S809

Savonius was placed in the middle of Darrieus rather than on top to save space. For this time, CFD was carried out in 2D because the turbine model in this study has a homogeneous shape from the bottom upwards.

Then, the boundary conditions are square with a + pattern in the middle of the boundary to make it easier to form a structured mesh. The size of the boundary condition refers to research [26], i.e., the turbine rotation center is 5D from the inlet side, 15D from the outlet side, 4D from the top and bottom, and the rotating zone has a diameter of 1.5D. D is the outer diameter of the turbine, which is the Darrieus diameter. The boundary condition is shown in Figure 3.

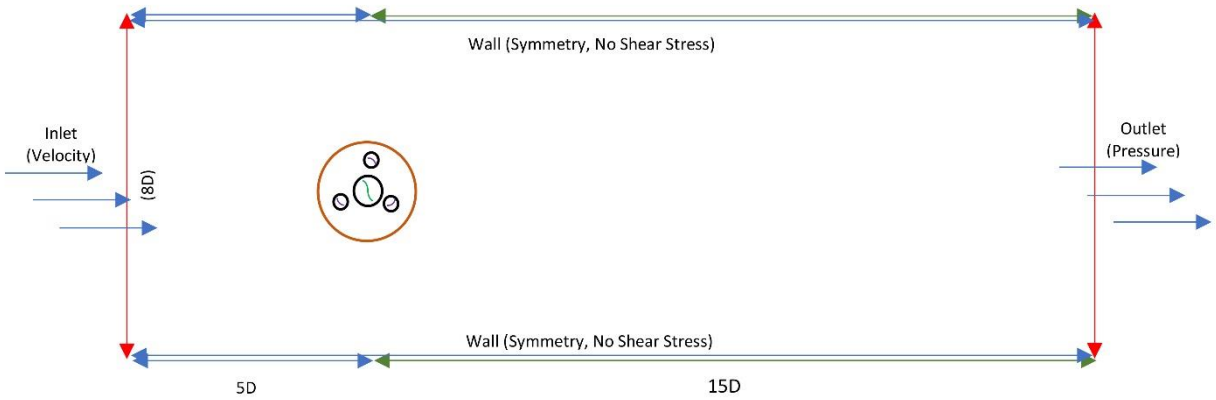

Figure 3 Boundary condition.

The velocity inlet is the area where the fluid enters. The rotating domain is the area where the turbine rotates. The outlet is the area where the fluid exits the domain. Thus, the fluid flows horizontally from the inlet to the outlet.

Then, the next stage is meshing. The mesh model is a hybrid mesh, a combination of structured and unstructured mesh [27]. It is attempted to make the number of structured mesh more than unstructured mesh. The mesh is arranged more tightly on the side of the turbine blade to capture the fluid phenomenon. Then, inflation is applied. The first layer thickness (Δs) is calculated using the following equation [20].

$$\Delta s = \frac{y^+ \mu}{U_f \rho} \tag{4}$$

y^+ is a non-dimensionless parameter, and the value is estimated to be 1, μ is the dynamic viscosity of air ($1.79 \cdot 10^{-5}$ kg/m·s), U_f is the velocity friction of turbine, and ρ is air density (1.225 kg/m^3). While the value of U_f is calculated using the following equation.

$$U_f = \sqrt{\frac{\tau_{wall}}{\rho}} \tag{5}$$

τ_{wall} is the wall shear stress which is calculated using the following equation.

$$\tau_{wall} = \frac{C_f \rho v^2}{2} \tag{6}$$

C_f is the skin-friction coefficient which is calculated using the following equation.

$$C_f = 0.079 Re^{-0.2} \tag{7}$$

Re is the Reynolds number which is calculated using the following equation [28].

$$Re = \frac{\rho U_\infty D_H}{\mu} \tag{8}$$

ρ is the density of the air (1.225 kg/m^3), μ is the dynamic viscosity ($1.7894 \cdot 10^{-5}$ kg/m·s) [29], U_∞ is the wind speed, D_H is the hydraulic diameter of the tunnel. The value of D_H is calculated using the following equation [30].

$$D_H = \frac{4ab}{a+b} \tag{9}$$

a is the tunnel width and b is the tunnel height. When a is 4.8 m, b is 0.46, and U_∞ is 5.3 m/s, the Reynold numbers value of the tunnel is $2.886 \cdot 10^5$. Then, the value of Δs can be obtained as 0.000103 m using Eq. 4. The meshing results are shown in Figure 4.

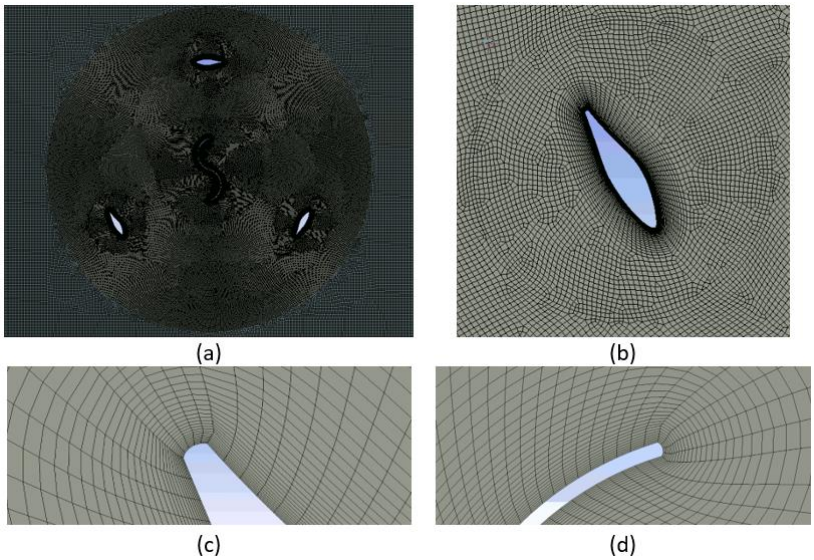

Figure 4 Meshing rotating zone (a), Darrieus blade (b), Darrieus tip (c), Savonius tip (d).

The efficient mesh density can be assessed through a grid independence test, which is a test that involves studying several variations of mesh density and selecting an efficient mesh model from these variations. The grid independence test method is used because this method is good enough to determine the effectiveness of the mesh composition in the computational process [31]. The mesh quality in this study is an average aspect ratio of 2.108, an average skewness of 0.001, and an average orthogonal quality of 0.996. Referring to [32], the mesh quality in this study is high enough for calculation analysis. However, validation must still be carried out using experimental data to ensure that the mesh density is truly acceptable.

2.2 Processing

The next stage is processing. The setup calculation used is shown in Table 2.

Table 2 Setup calculation.

Parameters	**Value**
Viscous model	Realizable k-e, Enhanced Wall Treatment
TSR	0.1 – 3.5
Turbine blade	Moving wall, rotational
Inlet	Velocity inlet (5.3 m/s)
Rotating zone	Rotated condition
Turbulent intensity	1%
Turbulent length scale	0.07D
Outlet	Pressure outlet
Boundary wall	Stationary wall, symmetry
Temperature	288.16 K
Ratio of specific heat	1.4
Solution method	SIMPLE, 2^{nd} order up wind, 1^{st} order implicit

A wind speed of 5.3 m/s was used because it was adjusted to the average wind speed in the ASEAN region [10] and the validation journal [33].

The selection of the viscous model and solution method in this study was carried out by trial and error to obtain the appropriate viscous model and solution method, which could give convergent results. The convergence is set at 10^{-4}, and data collection is carried out for the6th outer rotor rotations since the turbine starts rotating steadily after the 5th rotation.

The calculation process is carried out during this stage every 1° turbine rotation. According to [34], using an increment angle of 1° is recommended because it is quite accurate and does not take long. This affects the time step calculated using Eq. 9 [34].

$$\Delta t = \frac{\varphi}{180 \cdot \frac{\omega}{\pi}} \tag{10}$$

where Δt is the time step (s), φ is the azimuth angle (°), and ω is the rotating speed of the turbine rotor (rad/s).

Then, at this processing stage, the Moment Coefficient (C_M) value will be generated at each azimuth angle in each Tip Speed Ratio (TSR). To obtain the value of the total C_M in each TSR, the value of the C_M at each azimuth angle is averaged.

2.3 Postprocessing

The turbine Power Coefficient (C_P) is calculated manually using the following equation.

$$C_P = \lambda \cdot C_M \tag{11}$$

where λ is TSR that calculated from the outer rotor and C_M is Moment Coefficient. C_M values are displayed automatically from CFD results. Ansys calculates the C_M value using the Eq. 11.

$$C_M = \frac{T}{\frac{1}{4}\rho A D {U_\infty}^2} \tag{12}$$

where T is torque (N·m), ρ is air density (kg/m^3), A is rotor area (m^2), and U_∞ is air velocity (m/s). Finally, the C_M and C_P data are used to analyze the performance of the turbine.

3. Results and Discussion

3.1 Gird Independence Test

When performing CFD, the density of mesh elements greatly affects the accuracy of CFD results. The denser the mesh elements, the higher the C_P value. However, the high value of C_P does not mean that the CFD process is accurate. To determine the accuracy of the CFD results, it is necessary to validate them based on experimental data. A grid independence test is carried out to determine the configuration of mesh elements needed to provide accurate results and an efficient CFD process. The grid independence test uses the two-bladed Savonius model. After obtaining the correct ratio ratio configuration of the number of mesh elements, the configuration is carried out for the hybrid VAWT Savonius-Darrieus NREL S809 model. The mesh elements used for the grid independence test

in this study are 33097, 44949, 67759, and 113556, respectively. Setting the number of mesh elements is done by varying the size of the outermost mesh element sequentially by 3 cm, 2.8 cm, 2.6 cm, and 2.4 cm, then setting the ratio of the mesh element size to the inside of 0.5 from the outermost size. The process of the grid independence test is carried out on TSR 0.6 at a wind velocity of 5.3 m/s.

The grid independence test is evaluated through C_M and C_P graphs. Each graph shows the effect of increasing the number of mesh elements on the C_M and $C_P$values from the CFD results. The C_M graph at each azimuth angle from the results of the gird independence test is shown in Figure 5.

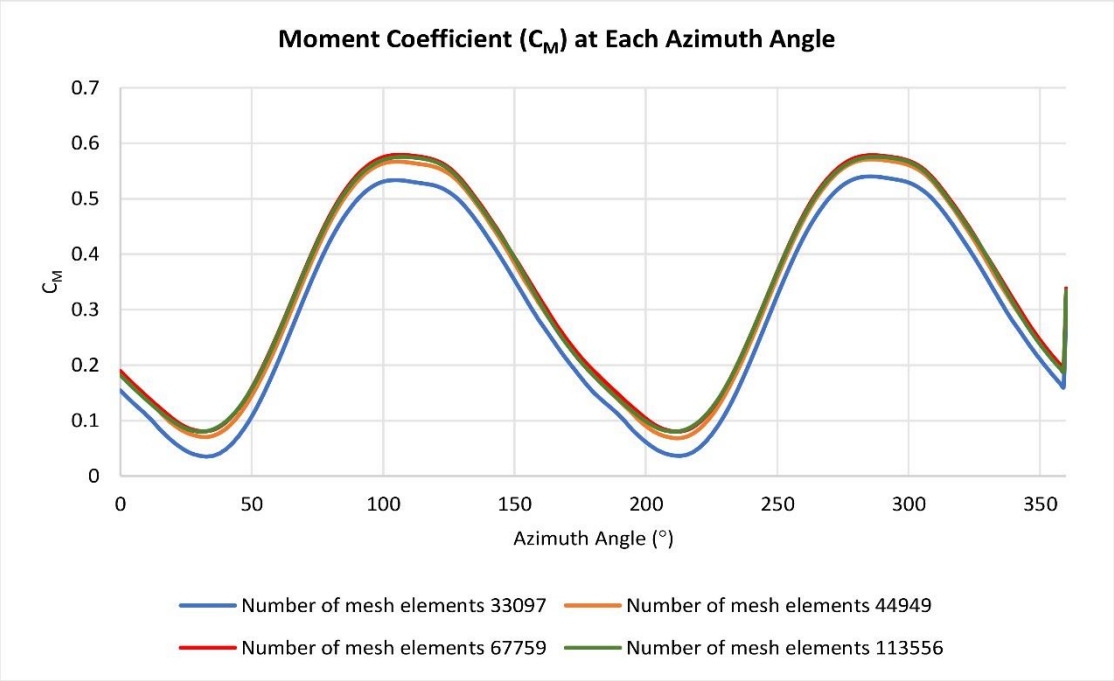

Figure 5 Graph of Moment Coefficient (C_M) at each azimuth angle.

Based on the graph in Figure 5, it can be observed that the more the mesh elements used, the higher the positive moment value in the turbine model, and vice versa. However, the higher resulting C_M value does not indicate accurate results.

Then, C_P data can be used to analyze the sensitivity level of the mesh to changes in the number of mesh elements given. The C_P data from the grid independence test is shown in Figure 6.

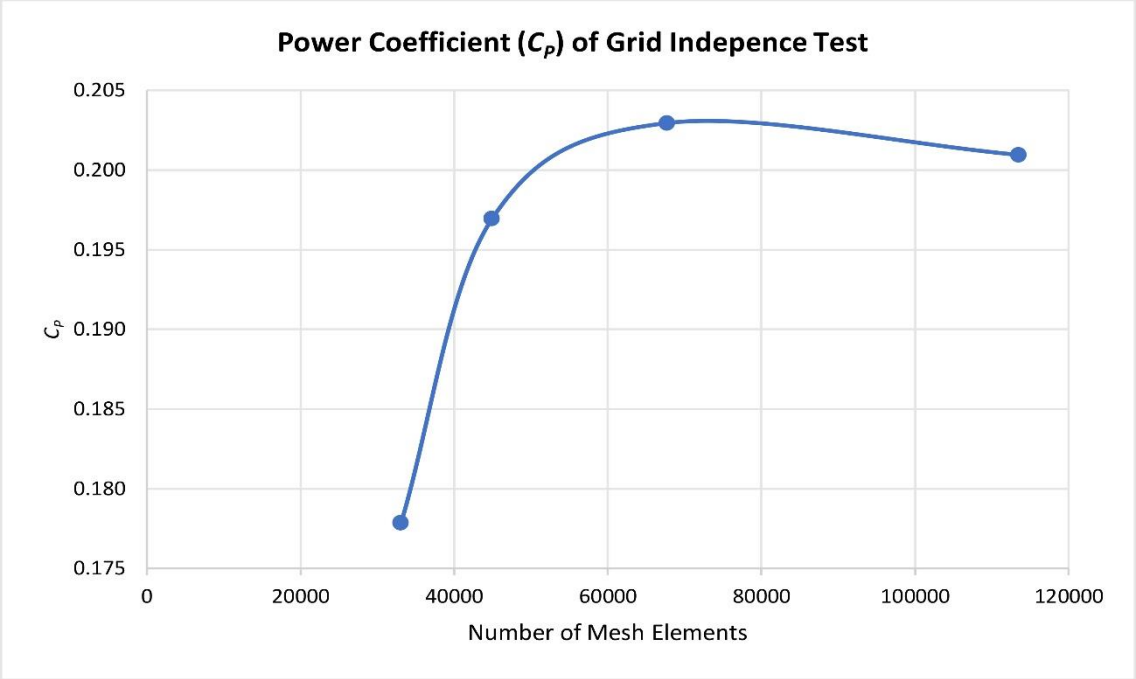

Figure 6 Power Coefficient (C_P) of grid independence test graph.

Based on the graph in Figure 6, the addition of the amount of mesh from 33097 to 44949 gives a large difference in the C_P value, which is 10.73%. It means that in this range, adding of the number of mesh still causes a significant change in the C_P value. The addition of the amount of mesh from 44949 to 67759 gives a C_P difference of 3.05%, while the addition of the mesh from 67759 to 113556 gives a very small difference, which is 0.99%. The slope of the graph of the change in C_P from the number of mesh elements 67759 to 113556 indicates that above the number of meshes 67759, the addition of the number of meshes no longer gives a significant difference to the C_P value. The more the number of mesh elements used, the longer the CFD process takes and the heavier the computer work becomes. Using the number of mesh elements 67759 is quite good in providing CFD results. The ${y^+}_{max}$ value for the internal rotor is 1.723, and the external rotor is 2.421. In addition, among all variations in the number of mesh elements used, the number of mesh elements 67759 has the smallest difference to the experimental data referring to [33], which is 5.82%. Therefore, the 67759-mesh density configuration is applied to the hybrid turbine CFD in this study.

3.2 Validation

The mesh density configuration obtained from the results of the grid independence test is used to validate the setup configuration. Validation is carried out to know the accuracy of the selected setup calculation. If the accuracy level is high enough, the selected setup calculation is appropriate and can be employed for the hybrid turbine model. The validation uses secondary data, namely the experimental data of the two-bladed Savonius turbine conducted by [33]. For the validation process, the dimensions of the two-bladed Savonius in this study are the same as the ones of research [33]. Validation is done at TSR 0.1 – 0.9 and wind velocity 5.3 m/s. The C_P graph of the validation results is shown in Figure 7.

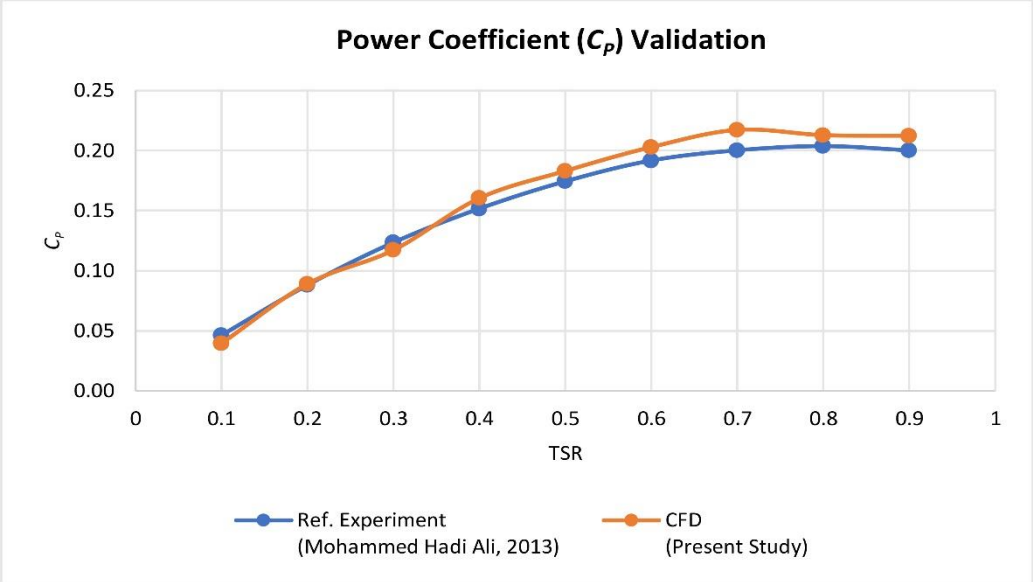

Figure 7 Power Coefficient (C_P) of the validation.

Figure 7 shows that the CFD data in this study is similar to the experiment's secondary data [33], except at high TSR, there is a slight difference in value. This slight difference occurs because although the dimensions of the turbine and several simulation conditions have been made the same as the reference, the temperature and pressure conditions used in the CFD are not the same as the reference since the factors such as the temperature and pressure of the test environment are not described in the reference. However, the Realizable k-e, Enhanced Wall Treatment viscous model in the CFD process provides an average difference of 6.26% against the secondary data of the experiment [33]. Based on research [35], the Realizable k-e, Enhanced Wall Treatment viscous model is recommended for hybrid VAWT CFD. Thus, it is believed that the setup calculations to validate the Savonius turbine also provide accurate results when implemented in a hybrid Savonius-Darrieus.

3.3 Velocity Distribution and Pressure Distribution

Free stream air flows into the turbine blade resulting in a collision between the air mass flow and the turbine blade. The collision causes a force on each turbine blade so that it can rotate it. Simultaneously, the airflow hits the returning blade and advancing blade of the Savonius. The advancing blade is the Savonius concave side facing the inlet while returning blade is the Savonius convex side facing the inlet. In principle, the advancing blade generates positive torque while returning blade generates negative torque. The torque generated by the advancing blade is more dominant so that the turbine can rotate.

Based on this CFD, the velocity contour can be seen in Figure 8.

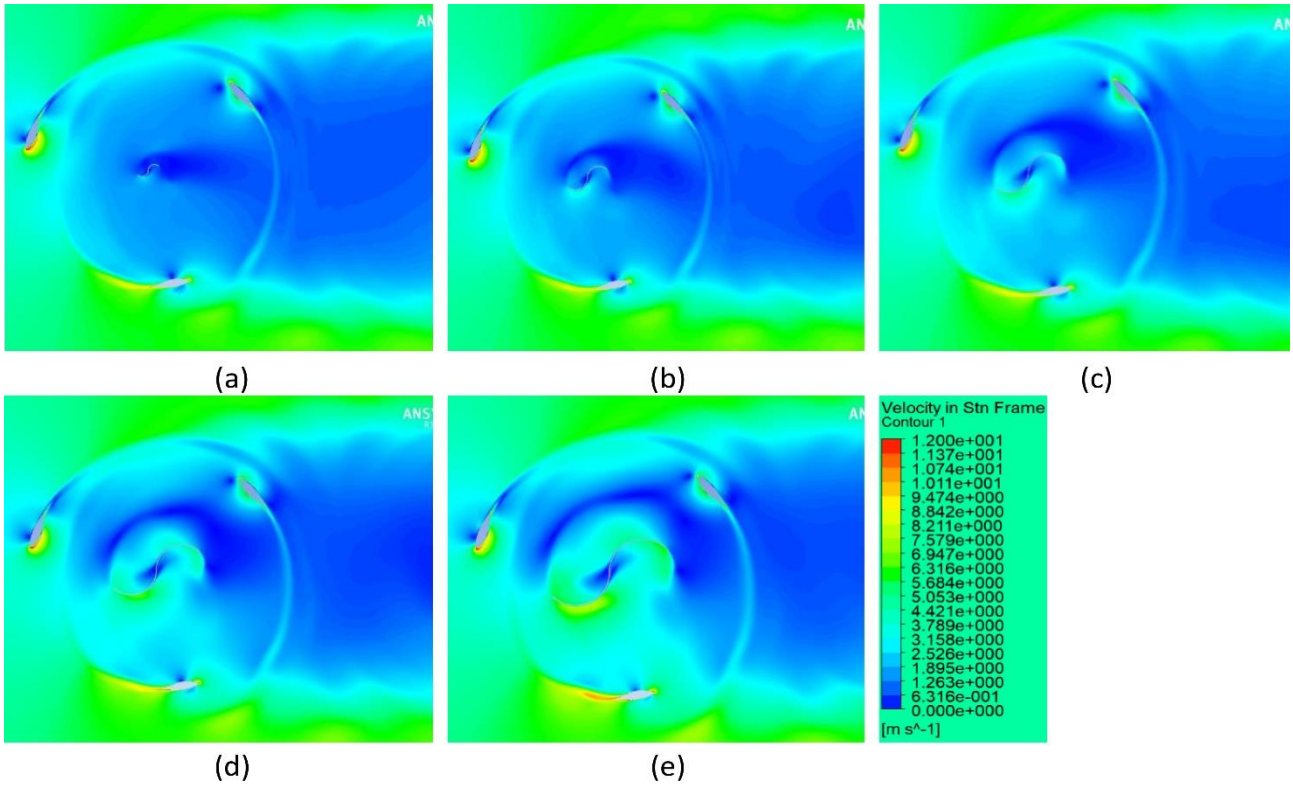

Figure 8 Velocity Contour of R_S/R_D 0.1 (a), R_S/R_D 0.2 (b), R_S/R_D 0.3 (c), R_S/R_D 0.4 (d), and R_S/R_D 0.5 (e).

The speed contour is taken at TSR 2.5 because it is the optimum TSR of the turbine. The velocity contours are shown at an azimuth angle of 115° because the different contours of each model are most clearly observed at that azimuth angle. Of the five models, the contour near the Darrieus airfoils is mostly the same, but there are differences on the Savonius side. The fluid velocity on the upstream side of Darrieus is lower than that on the downstream, and the greatest fluid velocity occurs at the leading edge. The flow velocity on the advancing side of the R_S/R_D 0.1 model is the lowest compared to the others. The blue contour color indicates this on the advancing blade model RS/RD 0.1, which is wider than the others. The highest fluid flow velocity on the Savonius advancing blade side occurs in the R_S/R_D 0.5 model. In addition, the flow rate behind the Savonius for the R_S/R_D 0.5 model is also the highest among the others. The flow velocity value is inversely proportional to the pressure so that if the flow velocity is low, the pressure at that point is high, and vice versa. This will be proven in the pressure contour analysis.

Then, the characteristics of the pressure generated by the turbine can explain the cause of the rotating turbine and produce a force value. The pressure contour that needs attention is the pressure difference around the turbine blade. The pressure contour of each turbine model is shown in Figure 9.

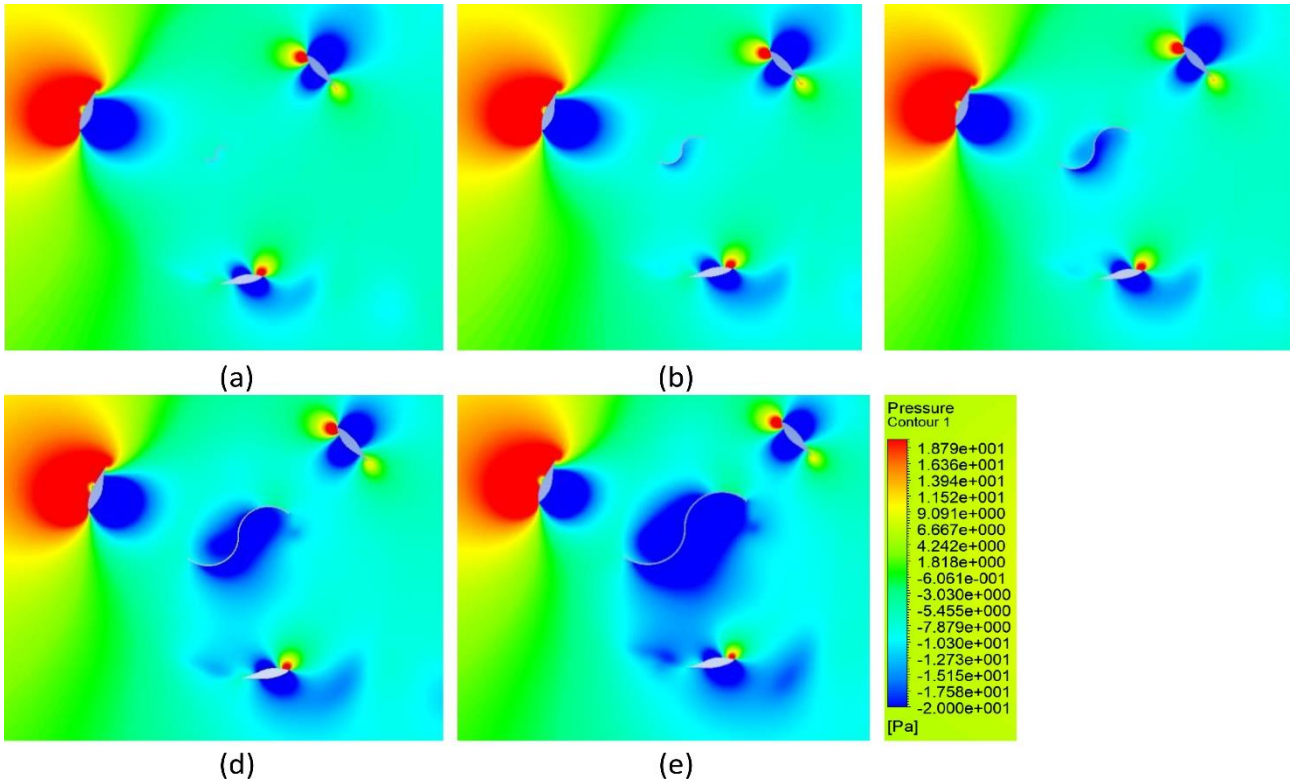

Figure 9 Pressure Contour of R_S/R_D 0.1 (a), R_S/R_D 0.2 (b), R_S/R_D 0.3 (c), R_S/R_D 0.4 (d), and R_S/R_D 0.5 (e).

The pressure contour is also presented at a TSR of 2.5 and an azimuth angle of 115°. Based on the picture in Figure 9, the pressure difference that occurs on Darrieus is greater than on Savonius. Darrieus's upstream side was under greater pressure than the downstream side. It is marked in red on the upstream side while blue on the downstream side. The pressure difference that occurs is very high, reaching 20 Pa upstream and -20 Pa downstream. A direct collision with the fluid mass flow from the inlet causes the high pressure on the upstream side of Darrieus. However, Darrieus's airfoil behind Savonius has a smaller difference than the other airfoils because the flow of fluid hitting it is blocked by Savonius.

Among all the models, the returning blade Savonius from the R_S/R_D 0.5 model receives the greatest pressure. This means that the negative torque generated by the R_S/R_D 0.5 model is the largest compared to the others. The turbine extracts the greater the negative torque that occurs, the less power. Meanwhile, the pressure difference in the Darriues airfoils of the five models tends to be the same. Thus, the R_S/R_D 0.5 model on the TSR 2.5 has the greatest negative torque, which can cause the power extracted by the turbine to be small. This is proven through the C_M and C_P graphs, which are discussed in the next section.

3.4 Moment Coefficient (C_M) and Power Coefficient (C_P) of Hybrid VAWT Savonius-Darrieus NREL S809

The essence of this study is to determine the effect of R_S/R_D on the performance of the hybrid VAWT Savonius-Darrieus NREL S809. This can be analyzed through C_M and C_P graphs from the CFD process. The C_M graph in each TSR is shown in Figure 10.

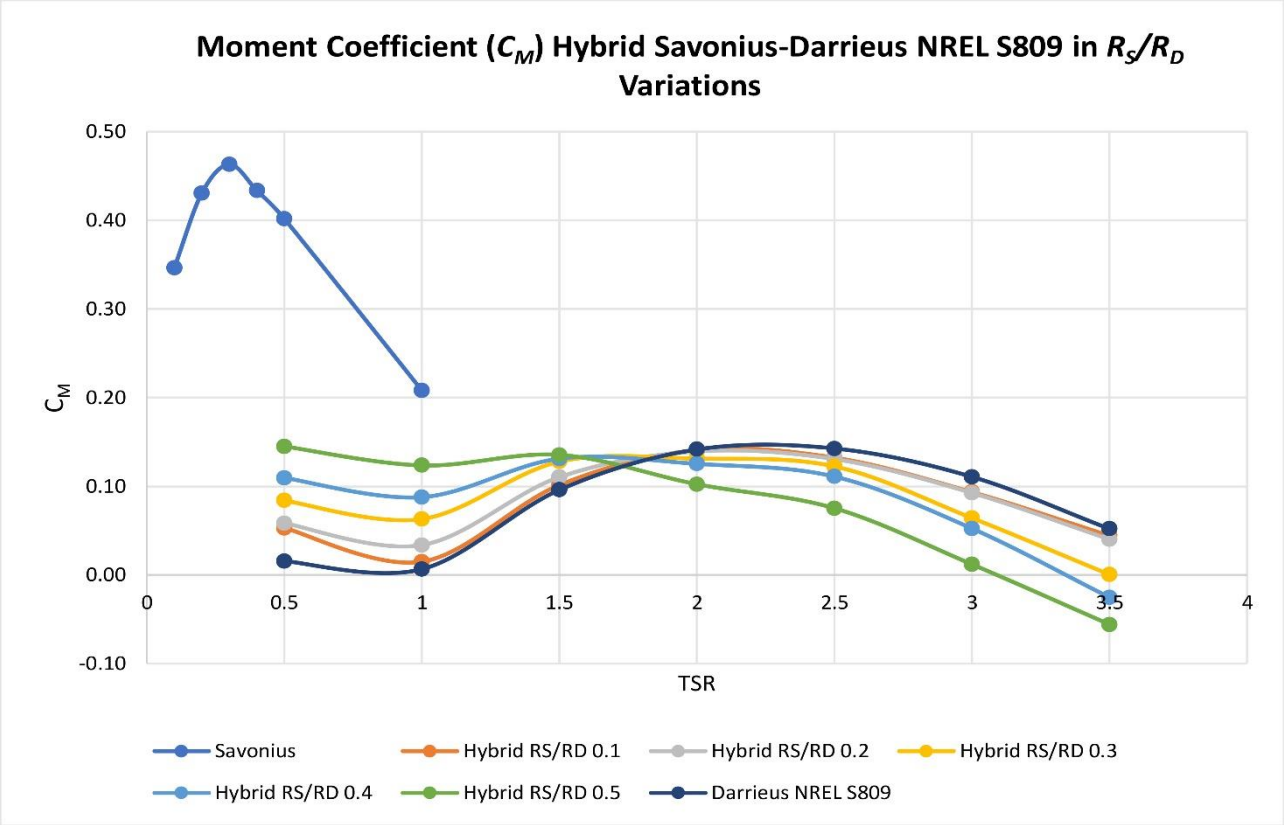

Figure 10 C_M graph in several R_S/R_D variations.

CFD is carried out in the TSR range of 0.5 -3.5 because in that range it can be observed the difference in each variation of R_S/R_D. The graph in Figure 10 shows that the greater the RS/RD value, the greater the CM value at low TSR. The high value of CM at low TSR The high value of C_M at low TSR means that the turbine has the sufficient self-starting capability.

Of all hybrid models, the C_M value at TSR 0.5 is greater than TSR 1. This is because Savonius works more dominantly at TSR less than 1. Darrieus works more dominantly in the next TSR, but Savonius inhibits Darrieus because it can't rotate at TSR above 1. As a result, after showing an increase in torque at a TSR above 1, at a certain TSR, all models show a decrease in C_M value again. A turbine owns the largest CM value at low TSR with an RS/RD of 0.5. This shows that the R_S/R_D 0.5 model has the best self-starting.

Furthermore, the wind speed required to rotate is also the lowest compared to the others. In the range of TSR 0.5 – 1.5, the C_M value of the R_S/R_D 0.5 model tends to be stable at C_M 0.15, though it is still unable to exceed the Savonius one. However, the C_M of the R_S/R_D 0.5 model is 8-times higher than single Darrieus at TSR 0.5 and the highest among all hybrid models; this value has exceeded the target to increase the initial C_M of the turbine, which is 5-times higher than a single Darrieus. At low TSR, the R_S/R_D 0.1 model has the smallest C_M value among the others. So, based on the graph of Figure 10, the increase in the R_S/R_D value does cause an increase in the initial C_M value of the turbine, but at a TSR above 1.5, the turbine shows a rapid decrease in C_M value.

Furthermore, when the C_M value is multiplied by the TSR as Eq. 10, the C_P value is obtained, as shown in Figure 11.

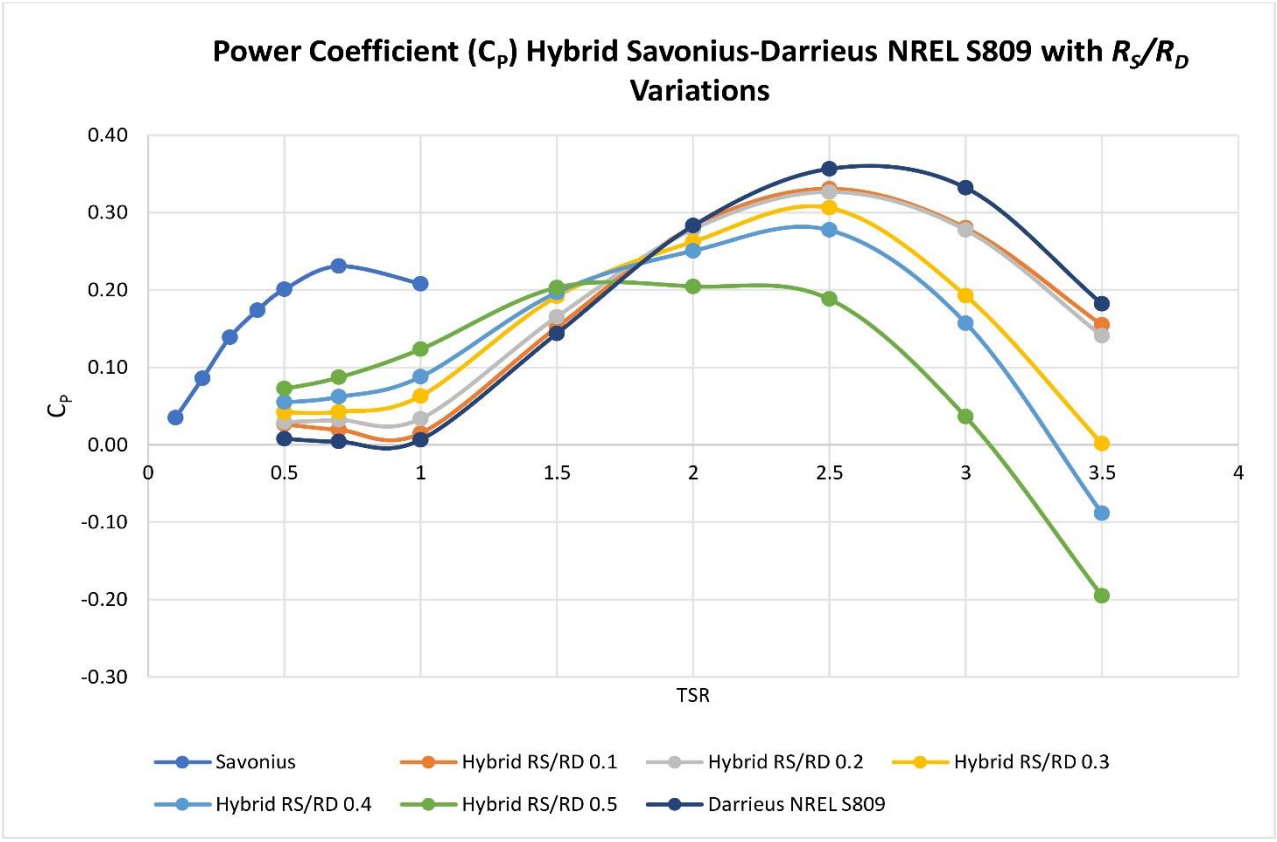

Figure 11 Power Coefficient (C_P) graph in several R_S/R_D variations.

The graph in Figure 11 shows that the greater the RS/RD value, the higher the CP value at the initial TSR. On the other hand, the greater the R_S/R_D value, the faster the C_P value drops at the TSR above 1.5, and the $C_{P_{max}}$ value is also getting smaller. Among all hybrid models, the highest $C_{P_{max}}$ value is owned by the 0.1 and 0.2 R_S/R_D models, which are 0.33 at TSR 2.5, respectively. The lowest $C_{P_{max}}$ value is owned by the R_S/R_D 0.5 model, which is 0.20 at TSR 1.5. The smaller the R_S/R_D value, the more dominant Darrieus's work is, which shows that the hybrid turbines with small R_S/R_D tend to have high C_P values at high TSR.

At initial TSR, the R_S/R_D 0.5 model has the largest C_P value of 0.07, while the R_S/R_D 0.1 model has the smallest C_P value of 0.03. However, at TSR above 1.5, the R_S/R_D 0.5 model experiences a rapid decrease in C_P value compared to other models. At TSR above 2, the hybrid model's CP can still not exceed a single Darrieus. Therefore, the R_S/R_D 0.5 model has the smallest $C_{P_{max}}$ value at high TSR compared to other models. However, the R_S/R_D 0.5 model has a C_P value 8-times higher than the single Darrieus in the initial TSR.

The Savonius Darrieus hybrid turbine's performance is a combination of each turbine's characteristics. Savonius has the characteristic of not being able to rotate above the wind that hits it. Based on these properties, since Savonius prevents Darrieus from rotating at a higher TSR, there is a decrease in the C_M and C_P value. However, as shown by Figs, based on the characteristics of each model. 10 and 11, the maximum advantage can be achieved if a turbine has C_M and C_P values as high as the R_S/R_D 0.5 model at the low TSR and as high as a single Darius at the high TSR. This condition can be obtained in several ways, one of which is by utilizing the rachet concept [36] so that at the low TSR, the turbine can rotate in hybrid mode, while at high TSR, the turbine is changed to a single Darrieus mode.

4. Conclusions

It can be concluded that increasing the Rotor Radius Ratio value has impacts the initial Moment Coefficient value of the hybrid VAWT Savonius-Darrieus NREL S809. When the Rotor Radius Ratio of the hybrid turbine is increased, the initial Moment Coefficient value also increases. However, the higher the Rotor Radius Ratio value, the lower the maximum Power Coefficient value. Among all models, Rotor Radius Ratio 0.5 has the best Moment Coefficient at low TSR but has the lowest maximum Power Coefficient. The Rotor Radius Ratio 0.5 model can increase the initial Moment Coefficient 8 times higher than the single Darrieus and 2 times higher than the Rotor Radius Ratio 0.1 model. Then, based on our findings, the maximum advantage can be achieved if a turbine has Moment Coefficient and Power Coefficient values as high as the Rotor Radius Ratio 0.5 model at the low TSR and as high as a single Darius at the high TSR.

Acknowledgments

The authors would like to thank Savry Chhin, Ikki Adji Dharma, Hanif Agha, and Elyas Nur Fridayana from Institut Teknologi Sepuluh Nopember, Surabaya, Indonesia for being a great discussion partners regarding CFD. We also thank the Department of Mechatronics and Artificial Intelligence, Universitas Pendidikan Indonesia, for providing computers during the data collection. Then, big thanks to the Shibaura Institute Technology, Tokyo, Japan for providing the fund to carry out this research.

Author Contributions

Elysa Nensy Irawan performed simulation study then evaluated the result, Sandro Sitompul advised how to improve the study regarding data collection and presentation, Ken-Ichiro Yamashita advised how to improve this study regarding installation of the machine, Goro Fujita organized the study progress toward publication including discrimination from other studies.

Funding

This research was funded by the Shibaura Institute of Technology, Tokyo, Japan.

Competing Interests

The authors have declared that no competing interests exist.

References

1. López-Sosa LB, Alvarado-Flores JJ, del Niño Jesús Marín-Aguilar T, Corral-Huacuz JC, Aguilera-Mandujano A, Rodríguez-Torres GM, et al. COVID-19 pandemic effect on energy consumption in state universities: Michoacan, Mexico Case Study. Energies. 2021; 14: 7642.
2. International Energy Agency. World Energy Outlook 2021. France: Directorate of Sustainability, Technology and Outlooks, International Energy Agency; 2021.
3. Bimanatya TE. Fossil fuels consumption, carbon emissions, and economic growth in Indonesia. Int J Energy Econ Policy. 2018; 8: 90-97.

4. Asif M, Muneer T. Energy supply, its demand and security issues for developed and emerging economies. Renew Sust Energy Rev. 2007; 11: 1388-1413.
5. Yoro K, Daramola MO. CO_2 emission sources, greenhouse gases, and the global warming effect. In: Advances in carbon capture. Cambridge: Woodhead Publishing; 2020. pp. 3-28.
6. International Energy Agency. Global Energy Review 2021: Assessing the effects of economic recoveries on global energy demand and CO_2 emissions in 2021. France: IEA; 2021.
7. Taibi E, Gielen D, Bazilian M. Renewable energy in industrial applications-An assessment of the 2050 potential. Vienna: United Nations Industrial Development Organization UNIDO; 2010.
8. Irawan EN, Saputro BP, Dharma IA, Warjono, Putra M, Muntini MS. An analysis of hybrid energy design for Yogyakarta International Airport (YIA). J Phys Conf Ser. 2021; 1951: 012032.
9. Balcioglu H, Soyer K, EL-Shimy M. Renewable energy–Background. In: Economics of variable renewable sources for electric power production. Saarbruecken: Lambert Academic Publishing/Omniscriptum; 2017. pp. 17-33.
10. Chang Y, Phoumin H. Harnessing wind energy potential in ASEAN: Modelling and policy implications. Sustainability. 2021; 13: 4279.
11. Li J. Wind power turbine system. In: CAD, 3D modeling, engineering analysis, and prototype experimentation. Cham: Springer; 2015. pp. 27-37.
12. Eftekhari H, Al-Obaidi ASM, Eftekhari S. Aerodynamic performance of vertical and horizontal axis wind turbines: A comparison review. Indones J Sci Technol. 2022; 7: 65-88.
13. Cheong SH, Choi SD, Shon JY, Mag-isa A, Kim SH, Choi MS. Improving the Self-starting Performance of a VAWT. J Korean Soc Manuf Process Eng. 2006; 5: 13-20.
14. El-Zafry AM, El-Hameed OE, Hassan MS, Shaheen MM. A review on the types of vertical axis wind turbines and the methods of their performance study. J Multidiscipl Eng Sci Technol. 2019; 6: 10633-10643.
15. El-Maksod I, El-Aal A, Hussein A, Hafez A, El-Attar A, Shahin A, et al. Performance analysis, design, and manufacturing of vertical axis wind turbine. Egypt: Alexandria University; 2018.
16. Wakui T, Tanzawa Y, Hashizume T, Nagao T. Hybrid configuration of Darrieus and Savonius rotors for stand-alone wind turbine-generator systems. Electrl Eng Jpn. 2005; 150: 13-22.
17. Ali NM. The effect of Darrieus and Savonius wind turbines position on the performance of the hybrid wind turbine at low wind speed. Int J Mech Eng Technol. 2020; 11: 56-72.
18. Abdolahifar A, Karimian SM. Aerodynamic performance improvement of hybrid Darrieus-Savonius vertical axis wind turbine. Amirkabir J Mech Eng. 2019; 52: 1865-1884.
19. Roshan A, Sagharichi A, Maghrebi MJ. Nondimensional parameters' effects on hybrid Darrieus-Savonius wind turbine performance. J Energy Resour Technol. 2020; 142: 011202.
20. Chhin S. Numerical simulations on hybrid Savonius-Darrieus wind turbine with varying airfoil shape and solidity ratio. Surabaya: Institut Teknologi Sepuluh Nopember; 2020.
21. Das Karmakar S, Chattopadhyay H. A review of augmentation methods to enhance the performance of vertical axis wind turbine. Sustain Energy Technol Assess. 2022; 53: 102469.
22. Puspitasari D, Sahim K. Effect of Savonius blade height on the performance of a hybrid Darrieus-Savonius wind turbine. J Mech Eng Sci. 2019; 13: 5832-5847.
23. Sahim K, Santoso D, Puspitasari D. Investigations on the effect of radius rotor in combined Darrieus-Savonius wind turbine. Int J Rotating Mach. 2018; 2018: e3568542.

24. Modi FN, Gilke NR. Computational analysis of various airfoil profile on the performance of H-Darrieus wind turbine. Proceedings of the 2018 IEEE International Conference on System, Computation, Automation and Networking; 2018 July 6-7; Pondicherry, India. Piscataway: IEEE.
25. Versteeg HK, Malalasekera W. An introduction to computational fluid dynamics: The finite volume method. 2nd ed. Harlow, England; New York: Pearson Education Ltd.; 2007. 503p.
26. Chhin S, Djanali VS. Numerical simulation on hybrid Savonius Turbine with NACA-Airfoils as H-rotor Blades. Proceedings of the 2020 International Seminar on Intelligent Technology and Its Applications; 2020 July 22-23; Surabaya, Indonesia. Piscataway: IEEE.
27. Sadrehaghighi I. Unstructured Meshing for CFD. 2022. Available from: https://www.academia.edu/44184149/Unstructured_Meshing_for_CFD.
28. Chanson H. 2-Fundamentals of open channel flows. In: Environmental hydraulics of open channel flows. Oxford: Butterworth-Heinemann; 2004. pp. 11-34.
29. Anderson JD. Fundamentals of aerodynamics. 6th ed. New York: McGraw Hill Education; 2017. 1130p.
30. Sahar AM, Wissink J, Mahmoud MM, Karayiannis TG, Ashrul Ishak MS. Effect of hydraulic diameter and aspect ratio on single phase flow and heat transfer in a rectangular microchannel. Appl Therm Eng. 2017; 115: 793-814.
31. Godderidge B, Tan M, Turnock S, Earl C. A Verification and validation study of the application of computational fluid dynamics to the modelling of lateral sloshing. Southampton, UK: University of Southampton; 2006; No 140.
32. ANSYS. ANSYS FLUENT 12.0 User's Guide-6.2.2 Mesh Quality [Internet]. Canonsburg, PA: ANSYS, Inc.; 2009 [cited date 2022 June 3]. Available from: https://www.afs.enea.it/project/neptunius/docs/fluent/html/ug/node167.htm.
33. Ali MH. Experimental comparison study for Savonius wind turbine of two & three blades at low wind speed. Int J Mod Eng Res. 2013; 3: 2978-2986.
34. Satrio D, Utama IK, Mukhtasor M. The influence of time step setting on the CFD simulation result of vertical axis tidal current turbine. J Mech Eng Sci. 2018; 12: 3399-3409.
35. Syawitri TP, Yao Y, Yao J, Chandra B. Assessment of stress-blended eddy simulation model for accurate performance prediction of vertical axis wind turbine. Int J Numer Method H. 2021; 31: 655-673.
36. Rizescu C, Baciu D, Rizescu D. Study behaviour of ratchet mechanism manufactured with 3D printing technology. IOP Conf Ser Mater Sci Eng. 2022; 1235: 012001.